International Journal of Multiphase Flow 35 (2009) 66–77

Contents lists available at ScienceDirect

International Journal of Multiphase Flow

journal homepage: www.elsevier.com/locate/ijmulflow

Numerical simulation of bubble formation on orifice plates with a moving contact line

Yuming Chen *, Rainer Mertz, Rudi Kulenovic

University of Stuttgart, Institute of Nuclear Technology and Energy Systems (IKE), Pfaffenwalding 31, Stuttgart 70569, Germany

ARTICLE INFO

Article history:
Received 4 January 2008
Received in revised form 4 June 2008
Accepted 25 July 2008
Available online 15 August 2008

ABSTRACT

The formation of bubbles on an orifice plate involves a moving contact line, especially in case of poor wetting conditions. The dynamics of the moving contact line and contact angle have a significant impact on the bubble departure size. Therefore, for the numerical simulation, an appropriate contact line boundary condition is essential for a correct prediction of the bubble formation. Numerical tests have been performed on two kinds of contact line models, one is a contact line velocity dependent model (Model-A, a commonly used model) and the other is a stick-slip model (Model-B). The calculation results using Model-A depend greatly on the prescribed maximum contact line velocity. With Model-B a parameter-independent prediction can be obtained provided that the mesh is sufficiently fine. The dynamic advancing and receding contact angles, which are two required inputs to both models, have a significant influence on the predicted bubble departure diameter, if the contact line moves beyond the inner rim of the orifice. The effect of wettability on the bubble departure size is realized via the variation of the maximum contact diameter. When the contact line sticks to a small region near the inner rim of the orifice, such as the bubble formation on a thin-walled nozzle, the effects of the contact angle and contact line models are negligible.

1. Introduction

The three-phase moving contact line is a fundamental problem for many industrial applications in multiphase flow. A material contact angle (given by Young's equation) can be defined at a position microscopically close to the contact line. Due to the hysteresis, there are many stable contact angles for a given system, of which the largest is called the advancing angle, the smallest the receding angle. When the contact line is moving, the dynamic contact angle differs from its equilibrium counterpart and can be beyond the range limited by the static advancing and receding angles (Sikalo et al., 2005; Marmur and Rubin, 1973; Chigarev and Chigareva, 1986; Schimann, 2004); it was found experimentally to depend on the static contact angle as well as on the capillary number $Ca = \mu u_{ct}/\sigma$, or even to depend on the flow field outside the contact line vicinity (Blake et al., 1999). There are also other factors which make the contact angle different from the static value (Kandlikar and Steinke, 2002; Drelich et al., 1996).

For engineering applications, the apparent contact angle is generally used as an auxiliary concept in studying the contact line dynamics, which is the angle formed between the wall and a line tangent to the interface at a certain (macroscopic) distance from the apparent contact line. Experimentally, the apparent contact angle is often determined using low-power optics at macroscopic scales (~0.01 mm). Due to the free-surface bending, the apparent contact angle by this definition is different from the angle microscopically close to the contact line.

Theoretically, by the no-slip boundary condition, the well-known stress singularity occurs at the contact line: the fluid velocity is finite at the free-surface but zero at the substrate. For partially wetting fluids, this contact line problem is typically addressed by either relaxing the no-slip boundary condition (with a slip model) or by accounting for the effects of the long range intermolecular van der Waals forces (disjoining pressure) (Diez et al., 2000). For completely wetting fluids, the inclusion of a microscopic precursor film in front of the apparent contact line removes naturally the singularity. The existence of the precursor liquid film under various wetting conditions is in debate. If it do exist, it is generally not fast enough to stay ahead of the contact line. Therefore, it is unlikely that these thin films provide a mechanism for relieving the stress singularity (Stoev et al., 1998).

For slip models, an independent specification of the contact angle as a boundary condition is needed for determining the free-surface shape. Classical approaches relate the contact angle to the contact line velocity (Ca) (Cox, 1986; Dussan et al., 1991). There exist a number of such theories (refer Shikhmurzaev, 1997, Section 9). A simplified form of these theories is the Tanner's law, which states that the apparent contact angle is proportional to $Ca^{1/3}$ as proved by some experiments for wetting fluids and at low speeds.

* Corresponding author. Tel.: +49 7247 824026; fax: +49 7247 823718.
E-mail address: yuming.chen@irs.fzk.de (Y. Chen).

0301-9322/$ - see front matter © 2008 Elsevier Ltd. All rights reserved.
doi:10.1016/j.ijmultiphaseflow.2008.07.007

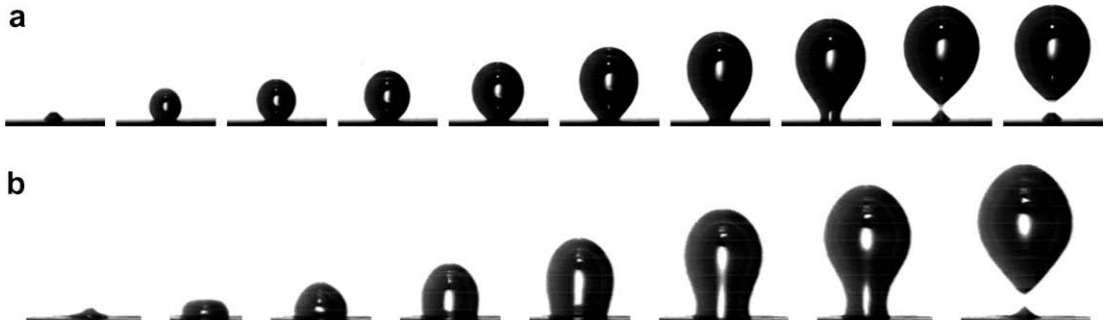

Fig. 1. Air bubble formation in water from orifice plates: (a) stainless steel surface (wetting); (b) stainless steel surface with wax coating (less wetting). Both the apparent contact angle and contact diameter vary throughout the growth period. For the poor wetting case, the contact diameter extends far beyond the orifice inner rim resulting in a much larger bubble size.

The Tanner's law suggests that the apparent contact angle involves a balance of capillary and viscous forces with intermolecular forces playing only a secondary role, particularly for $Ca > 10^{-5}$ (Kalliadasis and Chang, 1994).

Macroscopic numerical simulations[1] are widely used to study practical systems containing immiscible fluids with the main interest in macroscopic fluid and interfacial behavior. For these models, the apparent contact angle is specified as a boundary condition which is empirically related to the contact line velocity (slip velocity) (Smith et al., 2005; Huang et al., 2004; Francois and Shyy, 2003; Spelt, 2005). In studying droplet spreading, Sikalo et al. (2005) included a body force on the contact line which was determined from an empirical correlation relating the dynamic contact angle and contact line velocity (Ca) given by Kistler (1993). Therefore, the dynamic contact angle needs not to be prescribed. Mazouchi et al. (2004) implemented the so-called numerical slip in a boundary integral method for the free-surface Stokes flow. In this method, the domain was discretized in such a way that grid points occur near, but do not include the contact point, and the no-slip was enforced at all grid points along the solid substrate. The calculated interface profile was extended to the substrate at the specified (static) contact angle, determining the new contact line position. Thus in this case the grid spacing is equivalent to the slip-length. The calculation results (surface height, apparent contact angle) vary logarithmically with the grid spacing. Also the stability of the numerical scheme was found to depend strongly on the time step. The grid spacing used is of an order of 5 μm (the surface height is of an order of mm).

The major problem of these macroscopic simulations is that the simulation results depend on the slip-length and thus on the grid spacing (Mazouchi et al., 2004; Smith et al., 2005; Huang et al., 2004; Spelt, 2005; Renardy et al., 2001). As pointed out by Diez et al. (2000), the slip model with a constant slip-length is not viable from the numerical point of view, since it requires an extremely small grid spacing. According to Somalinga and Bose (2000), the theories from Cox (1986) and Dussan et al. (1991) are able to provide a physical boundary condition for the contact angle for negligible Reynolds numbers. Unfortunately, even the outer region considered in the theories, where the capillary forces dominant, is still much smaller than the commonly affordable mesh size (Sikalo et al., 2005). Furthermore, these theories are for small capillary numbers and negligible Reynolds numbers. Due to the lack of physical boundary conditions, in some studies the measured dynamic contact angle was directly used as a boundary condition, e.g., Pasandideh-Fard et al. (1996), Fukai et al. (1995).

The formation of bubbles on a solid surface also involves a moving contact line, but receiving far less attention compared to the droplet problems. In case that a bubble is formed on a thin-walled nozzle, the contact line can stick to the nozzle inner or outer rim while the contact angle can vary well beyond the limits given by the receding and advancing angles (Marmur and Rubin, 1973), the behavior of the moving contact line has little impact on the bubble departure diameter (Oguz and Prosperetti, 1993). The same is true for bubble formation under liquid co-flow conditions (Chen et al., 2008). However, in case that a bubble is formed on a plane surface such as an orifice plate, both the apparent contact angle and the contact diameter vary in a complicated manner as the bubble grows in size (see Fig. 1 and the figure caption). There is no universal pattern of the time-history of the contact angle and contact diameter (refer experimental results given by Chigarev and Chigareva (1986), Schimann (2004), Kandlikar and Steinke (2002), Gnyloskurenko et al. (2003) and Duhar and Colin (2006)). In this case, the bubble departure diameter is strongly influenced by the contact line behavior, which depends partially on the surface wettability (Gnyloskurenko et al., 2003).

Obviously, in order to predict accurately the bubble departure diameter in most situations, the moving contact line has to be included in the theoretical formulation. The traditional predictions based on the force balance at a certain time point are barely successful (Fritz, 1935; Jensen and Memmel, 1986).[2] Most of the numerical simulations on gas bubble formation on submerged orifices were carried out either using non-spherical models (interfacial element method) (Marmur and Rubin, 1976; Liow and Gray, 1988) or using rigorous boundary integral methods (Oguz and Prosperetti, 1993; Xiao and Tan, 2005). The latter is applicable only to a restricted type of flow problems, e.g., potential or Stokes flows. Very few studies are available by solving the full Navier–Stokes equations, e.g., Gelach et al. (2007), perhaps due to the high computational costs. Only a few numerical studies have taken into account the effects of moving contact line, e.g., Liow and Gray (1988). In the study of Gelach et al. (2007), a constant contact angle was used to study the effects of wettability.

In case of boiling on a heated surface, which is an important field of engineering applications, the mechanisms governing the moving contact line underneath a growing vapor bubble are further complicated by the evaporation on the bubble base and the

[1] By "macroscopic", we mean that the length scale is of an order of 1–100 μm, which corresponds to the commonly affordable numerical or visualization resolution. Therefore, the contact angle in this case is apparent. In fact, if the length scale is less than 1 μm, for many technical surfaces with a surface roughness of around 1 μm, the 3D surface topography has to be taken into account. This is certainly a formidable task.

[2] The concept of using force balance to predict the bubble departure diameter is not correct, since according to the Newton's second law, the net force on the bubble should be zero all the time. The predictions were actually achieved by an *incomplete* force balance, making use of different magnitudes of various forces at different growth stages.

non-uniform temperature field, resulting the Marangoni flows, vapor recoil forces, etc. There are several numerical studies on the formation of isolated boiling bubbles (Stephan and Hammer, 1994; Son et al., 1999). All these studies consider an evaporating microlayer and a non-evaporative thin film beneath the bubble. According to Son et al. (1999), for a given dispersion constant, the calculated apparent contact angle is "nearly independent of the bubble growth process", which implies that the applied contact line model (including the long range van der Waals forces) may not be appropriate. Very recently, Mukherjee and Kandlikar (2007) studied the effects of dynamic contact angles on single bubble formation during nucleate boiling using two kinds of contact line models without considering the microlayer evaporation.

Apparently, for a relatively long period of time, the macroscopic methods will be still dominant in studying the multiphase flow phenomena with a moving contact line, both experimentally and numerically. Therefore, it is important to have a detailed numerical assessment of the commonly used contact line models and to find a parameter-independent contact line model. These are done in this numerical study in the context of bubble formation on submerged orifices. Furthermore, the effects of contact angle will be discussed in details.

2. Numerical scheme

In this study, the unsteady, incompressible Navier–Stokes equations have been solved for 2D axisymmetric laminar flows. The calculation domain is a half cylinder (Fig. 2). A level set method developed by Osher and Sethian (1988) is used to track the two-phase interface.

2.1. Level set method

In the level set method, a continuous function ϕ is introduced over the whole computational domain. This level set function is given the property of a distance function indicating the shortest distance to the interface. Thus, the zero level set of the function ($\phi = 0$) represents the interface. We take $\phi < 0$ in the gas region and $\phi > 0$ in the liquid region. The evolution of ϕ is given by

$$\frac{\partial \phi}{\partial t} + \vec{w}\cdot\nabla\phi = 0, \tag{1}$$

where $\vec{w}$ is the velocity of the interface. The physical properties are assumed constant in each fluid, they take different values depending on the sign of ϕ. To avoid a sudden jump of the material properties across the interface, which can have a substantial effect on the stability of the numerical scheme, a smoothed Heaviside function is defined

$$H(\phi) = \begin{cases} 0 & \text{if } \phi < -\varepsilon \\ 0.5[1 + \phi/\varepsilon - \sin(\pi\phi/\varepsilon)/\pi] & \text{if } |\phi| <= \varepsilon \\ 1 & \text{if } \phi > \varepsilon \end{cases} \tag{2}$$

with $\varepsilon = 3h/2$ (h is the grid spacing). A smoothed material property γ, e.g., density, viscosity, etc., is then calculated by

$$\gamma(\phi) = \gamma_L H(\phi) + \gamma_V(1 - H(\phi)). \tag{3}$$

The initial value of ϕ can be chosen to be a distance function, however under the evolution of Eq. (1) it will not necessarily remain one. Thus it is necessary to reinitialize ϕ so that it remains a distance function without changing its zero level set. We use the redistance techniques proposed by Sussman and Fatemi (1999). The mass loss (or gain) is the main problem for the level set method in certain situations, e.g., in studying free rising bubbles. In this study, the rate of mass loss is negligible (less than 1%) compared to imposed gas flow rate, therefore it is not a least concern.

2.2. Governing equations

The non-dimensional governing equations are

$$\nabla\cdot\vec{w} = 0, \tag{4}$$

$$\frac{\partial \vec{w}}{\partial t} + \frac{\nabla p}{\rho} = -\vec{w}\cdot\nabla\vec{w} + \frac{1}{Fr}\vec{g} + \frac{1}{\rho Re}\left[\nabla\cdot(\mu\nabla\vec{w}) + \nabla\cdot\left(\mu\nabla\vec{w}^{T}\right)\right] + \frac{\kappa\delta\nabla\phi}{\rho We} = F^{n}. \tag{5}$$

Here a continuous surface force model is used (refer Brackbill et al., 1992). In Eq. (5), δ is a delta function given by the relation $\nabla H = \delta\nabla\phi$. The Navier–Stokes equations are solved using the projection method of Chorin (1968). In this method an intermediate velocity field $\vec{w}^{*}$ is first calculated, which is generally not divergence free, then the pressure at the next time level is calculated that ensures the velocity field satisfying the continuity equation.

2.3. Discretization

A finite difference scheme is applied on a 2D staggered (MAC) grid system with an equal grid spacing h. In this grid system, the pressure and level set function are defined at cell centers (i,j), while the velocities are defined at the cell faces, viz. $u_{i+1/2,j}$ and $v_{i,j+1/2}$. A fifth order WENO scheme (Shu, 2003) is adopted for the treatment of the convection terms in the momentum equations (Eq. (5)) and the advection equation for the level set function (Eq. (1)). The viscous and curvature terms are discretized using a central difference scheme. A Bi-CGSTAB method with ILU preconditioner is employed for solving the discretized Poisson equation.

The maximum allowable time step $\Delta t_{\max}$ is determined by restrictions due to CFL condition for explicit schemes. The real time step Δt is obtained by

$$\Delta t = C_t \Delta t_{\max}. \tag{6}$$

Here C_t(<1) is a coefficient. In this study, C_t is given as a constant value in each calculation during most of the bubble formation period. An adaptive time step is used for the 100 steps before and after

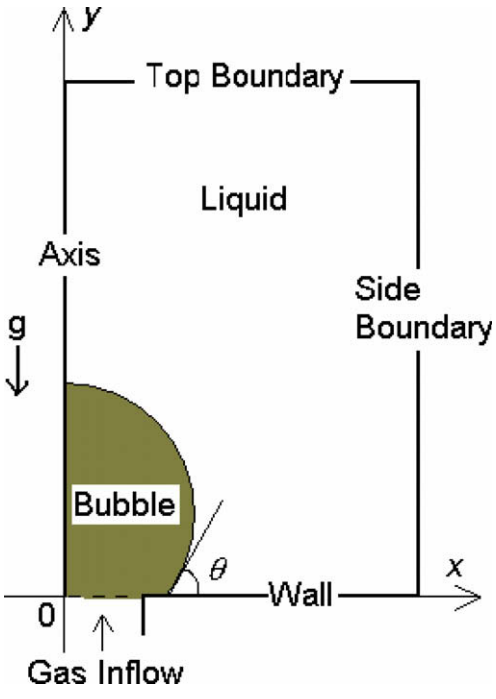

Fig. 2. Calculation domain.

bubble detachment where C_t is set to approach a minimum as bubble approaches detachment. Without this treatment, the calculation can break down during the bubble detachment stage in some cases.

2.4. Initial and boundary conditions

For the initial conditions, the two velocity components are set to zero. The initial bubble is set to be a hemisphere centered on the middle of the orifice mouth, thus the initial level set function can be easily determined. Symmetric condition is used for the level set function at the axis and the side boundary. An interpolation scheme is used for the wall and top boundaries. For the velocity boundary conditions, we apply symmetric conditions on the axis and the side boundary, out-flow conditions on the top boundary, inflow conditions at the orifice inlet. For the orifice wall, the no-slip ($L_s = 0$), Navier-slip ($u_{slip} = -L_s(\partial u/\partial y)|_{wall}$), free-slip ($L_s = \infty$) and local-free-slip conditions are tested. By local-free-slip, the free-slip is applied on the contact line position and the slip velocity is gradually reduced to zero as the horizontal distance from the contact line increases to 5 h, beyond a distance of 5 h no-slip condition is applied.

2.5. Contact line models

Special treatment of the contact line movement is needed due to the hysteresis and the dynamic nature of the contact angle. Two kinds of contact line models are used.

2.5.1. Model-A (contact line velocity dependent model)

In this model, the apparent contact angle is linearly related to the contact line velocity (u_{ct}). In addition, the Navier-slip condition is applied on the wall. This kind of models has been commonly used for macroscopic simulations (Smith et al., 2005; Huang et al., 2004; Francois and Shyy, 2003; Mukherjee and Kandlikar, 2007). In this calculation, similar to the procedure given by Francois and Shyy (2003), the instantaneous apparent contact angle θ is set to vary linearly between the prescribed receding angle θ_{re} and the advancing angle θ_{ad} if the instantaneous contact line velocity u_{ct} is within a given maximum, $\pm u_{ct,max}$. Beyond this range, the contact angle is assigned by the value of θ_{ad} or θ_{re}, depending on the sign of contact line velocity, namely

$$\theta = \begin{cases} \theta_{re} & \text{if } u_{ct} < -u_{ct,\,max} \\ \theta_{re} + (\theta_{ad} - \theta_{re})\frac{u_{ct}+u_{ct,\,max}}{2u_{ct,\,max}} & \text{if } |u_{ct}| <= u_{ct,\,max}\,. \\ \theta_{ad} & \text{if } u_{ct} > u_{ct,\,max} \end{cases} \tag{7}$$

At the inner rim of the orifice wall, the contact angle is allowed to have any value between θ_{re} and 180°. Physically, the orifice edge is generally rounded (not in an ideal right angle), the apparent angle can be up to a value of $(90° + \theta_{ad})$. Numerically, this condition prevents the contact line to recede into the orifice. The contact line velocity is obtained by interpolating from the velocities of the first two layers of cells next to the wall.

We found that the direct use of the above scheme imposes a severe time step restriction and requires a high mesh resolution. Furthermore, the relationship between the contact line velocity and the contact angle prescribed by Eq. (7) could cause unphysical behavior of the contact line movement, viz. the contact point can move backwards even when the contact line velocity is positive, or vice versa. Therefore, further restrictions are imposed: when the contact line velocity is positive while the contact point moves backwards, the contact line position is set to the same position as in the former time step, and the contact angle is recalculated accordingly. The same procedure is used for the opposite case.

In fact, the above model is only partially justified. In a droplet impingement experiment, Bayer and Megaridis (2006) showed that, for partially wetting surfaces, both the advancing and receding contact angle approach to a constant if the absolute contact line velocity increases beyond a certain value. For the receding case, this velocity is about 0.1 m/s, while it is about 0.3 m/s for the advancing case. The relationship between u_{ct} and θ was found to depend on surface wettability, impact velocity and different spreading–receding cycles. Pasandideh-Fard et al. (1996) showed a (constant) maximum advancing contact angle of approximately 110° when the contact line velocity reaches about 0.2 m/s. As already pointed out in the introduction, a contact line model similar to Model-A could lead to a simulation result depending on the slip-length and grid spacing. Therefore, it is important to develop a numerically independent model.

2.5.2. Model-B (stick-slip model)

Model-B is basically a kind of hypothesis. It has not yet been justified by experiments or theories. In this model, the instantaneous apparent contact angle is also limited by the prescribed values of the apparent receding and advancing contact angles, except when the contact line sticks on the orifice rim. However, there is no explicit relationship between θ and u_{ct} as given by Eq. (7). The variations of the contact angle and contact line position are shown schematically in Fig. 3. Assuming that the initial interface is $a - b$ (l.h.s of Fig. 3), when the interfacial velocity at a distance h (one grid spacing) from the wall is positive, viz. interface point moves from b to c after a time step Δt, the contact point tends to remain

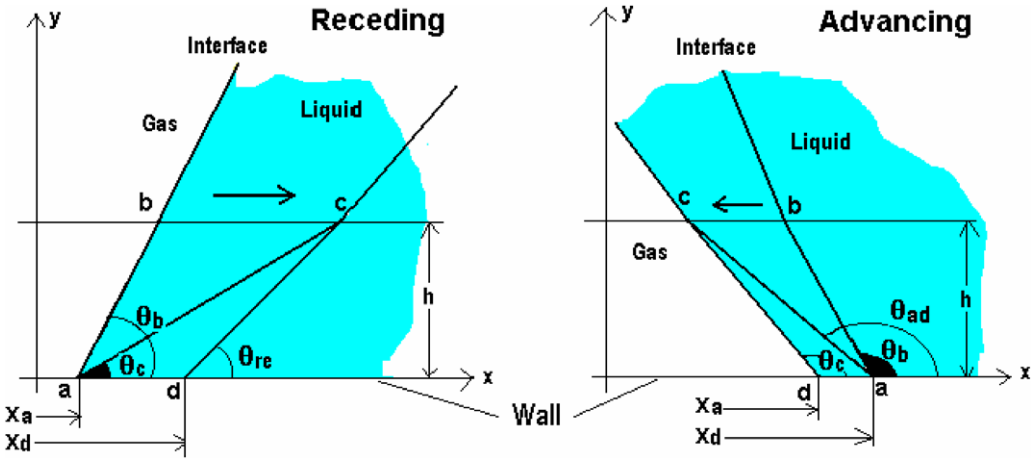

Fig. 3. Contact line Model-B (stick-slip model).

at the point a due to hysteresis. Thus the contact angle will change from θ_b to θ_c. However, if $\theta_c < \theta_{re}$, the contact line position will move from a to d while the contact angle will be equal to θ_{re}. The contact angle and contact line position for an advancing meniscus can be determined in a similar way (r.h.s of Fig. 3).

2.5.3. Numerical implementation of contact line models

We tested three methods in implementing the contact line models. In the first method, for each time step after the advection of the level set function by Eq. (1), the contact line position and/or contact angle are brutally adjusted according to the contact line models. The adjustment is repeated once more after the re-distance operation of the level set function. In the second method, the re-distance, contact line adjustment and projection operations are iterated for three times. The calculation results are essentially the same as for the first method. In the third method, we tested an iteration technique similar to the one used by Spelt (2005), where the contact line model is implemented at each pseudo time step in the re-distance operation (typically two to three steps). We found that the resulted variation of the contact angles from the last two steps is less than 0.001–0.01°. Although the calculated bubble departure diameter is slightly different from that by using the first method, the parameter dependencies are similar to those shown in Section 3.2. The data shown in this paper are all obtained by using the first method.

3. Results and discussion

Except for Section 3.1, the calculation examples shown in this paper are for the formation of adiabatic air bubbles from a single orifice or nozzle submerged in a water pool with constant gas flow rates. The fluid properties are taken at a temperature of 20 °C. Unless otherwise stated, the results are shown only for the first detached bubble for each calculation. The bubble departure diameter is the key parameter characterizing a given bubbling system; therefore, it will be the center of the following discussions.

3.1. Verifications

The numerical scheme has been tested for gas bubble formations on a thin-walled nozzle with or without liquid co-flow where the contact line tends to stick on the inner rim of the nozzle. The predicted bubble formation time is in very good agreement with the experiments (Chen et al., 2008). For the cases where the contact line could move back and forth, we verify the numerical model with a droplet relaxation problem.

In this test, a hemispherical water droplet with an initial contact radius of R_0 is placed on a horizontal surface in the ambient air. The droplet adapts its shape until the equilibrium state is achieved. The steady-state solution of the problem depends on the static contact angle θ_s and the Eotvos number ($\mathrm{Eo} = \rho_L g R_0^2/\sigma$) which is the ratio of the gravity force and capillary force. For $\mathrm{Eo} \ll 1$, the shape of the droplet is controlled by the capillary force and shows a shape of spherical cap. The maximum height of the droplet, H_0, is given by

$$H_0 = R_0(1-\cos\theta_s)\sqrt{\pi/(2\theta_s - 2\sin\theta_s\cos\theta_s)}. \tag{8}$$

For $\mathrm{Eo} \gg 1$, the shape of the droplet is controlled by the gravity force and the maximum height of the droplet, H_∞, is proportional to the capillary length (Dupont et al., 2007):

$$H_\infty = 2\sqrt{\sigma/(\rho_L g)}\sin(\theta_s/2). \tag{9}$$

Fig. 4 shows the normalized steady-state droplet height against the Eotvos number. The contact line Model-A is used in the calculations with $\theta_{ad} = 110°$ and $\theta_{re} = 100°$. The initial water droplet radius ranges from 0.1 to 10 mm, corresponding to an Eotvos number of 0.00135 and 13.5, respectively. The normalized droplet height agrees well with the two asymptotic solutions of Eqs. (8) and (9) for $\mathrm{Eo} \ll 1$ and $\mathrm{Eo} \gg 1$, respectively. For $\mathrm{Eo} = O(1)$, the transition between the spherical cap and the puddle occurs.

The results of parametric dependency study are shown in Fig. 5 in terms of relative deviations in the calculated droplet height as compared to a reference case described inside the figure. The initial

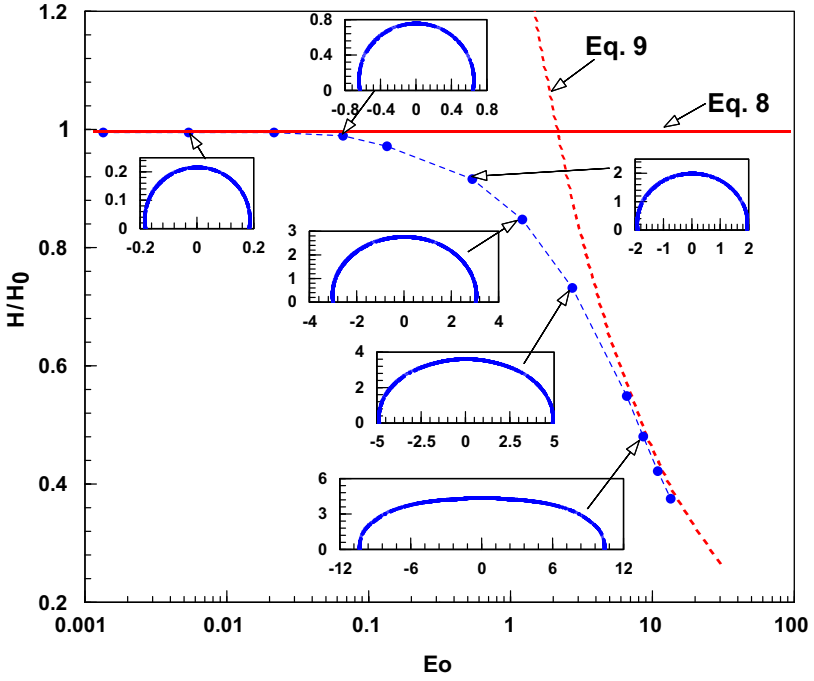

Fig. 4. Normalized droplet height against the Eotvos number (water, Model-A, $\theta_{ad} = 110°$, $\theta_{re} = 100°$, $U_{ct,max} = 0.1$ m/s, $L_s = 2$ h, wall BC: local-free-slip).

droplet radius is 1 mm for these calculations. The maximum deviation is about 1.8% when the prescribed maximum contact line velocity is larger than about 0.25 m/s; below this value, there is no change in the calculated droplet height. The grid spacing h also influences the calculations results. The relationship between the droplet height and h is nonlinear. The effect of slip-length is small. By using the contact line Model-B, the calculated droplet height is only slightly smaller than that using Model-A. No impact or negligible impact is shown for the domain size and time step size. Compared to the parameter-dependent study to be shown in Section 3.2 for gas bubble formation, parameter dependency for the droplet relaxation is generally much weaker.

3.2. Parameter dependency

The dependency of the numerical schemes adopting the contact line Model-A and Model-B on various parameters are discussed in this section for bubble formation. The orifice diameter D_o is 2 mm and the gas flow rate Q is 3 cm^3/s. The advancing contact angle is set to 110° and the receding angle 40°. The Navier-slip is used as the wall boundary condition with a slip-length of 2 h.

3.2.1. Effect of grid spacing h (Fig. 6)

For D_o = 2 mm and Q = 3 cm^3/s, the bubble departure diameters calculated by using the contact line Model-A and Model-B converge to a single value for a grid spacing less than 0.07 mm/grid and the change of bubble diameter with grid-size is rather small. In this calculation a grid-size independent result has not yet been obtained. For the case D_o = 1 mm and Q = 1 cm^3/s, the deviation between Model-A and Model-B are much bigger than the former case. The deviation becomes smaller as h decreases. For Model-B with h< = 0.09 mm/grid, the discrepancies are generally small by using the Navier-slip (with L_s = 2 h) and the local-free-slip conditions; the calculation results tend to converge with regarding to the grid-size. By using Model-A, the discrepancies are relatively big between a slip-length of 0.5 and 2 h. Overall, the predictions for the case D_o = 1 mm and Q = 1 cm^3/s are more unreliable. Thus the parameter studies shown follows are carried out for D_o = 2 mm and Q = 3 cm^3/s.

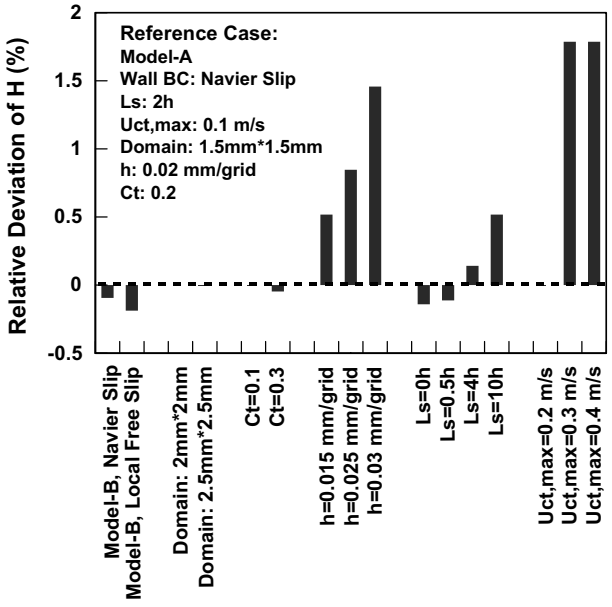

Fig. 5. Relative deviations of calculated droplet height by using different parameters (initial droplet radius: 1 mm).

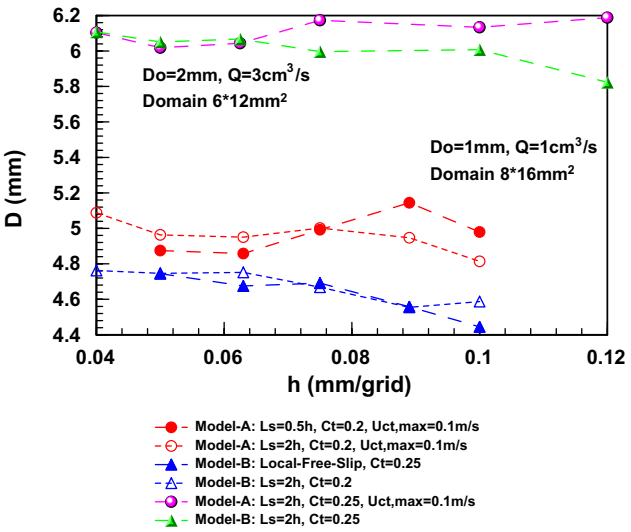

Fig. 6. Effect of grid spacing.

3.2.2. Effect of time step (Fig. 7)

In general, the applied time step size is of an order of microseconds, which is subjected to the CFL conditions and is progressively smaller as the bubble approaches detachment, because we use an adaptive time step scheme to ensure the numerical stability. For Model-B, the time step size has essentially no impact on the calculation results. For Model-A with h = 0.0625 mm/grid, the convergence is achieved at C_t< = 0.25; however, for h = 0.075 mm/grid, the calculated bubble diameter is found to depend nonlinearly on C_t.

3.2.3. Effect of slip-length L_s (Fig. 8)

By using the Navier-slip condition on the wall, the slip-length L_s has to be prescribed. When L_s is zero, it is equivalent to the no-slip condition; when L_s approaches infinity, it is equivalent to the free-slip condition. For Model-B, the slip-length has essentially no influence on the departure diameter. For Model-A with h = 0.075 mm/grid, the calculated bubble diameter is found to depend nonlinearly on L_s in the entire range of L_s. With h = 0.0625 mm/grid, the calculation results do not depend on L_s when L_s> = 5 h. This is in accordance with the conclusion of Spelt (2005) that the slip-length should be sufficiently large compared to the grid spacing in order to minimizing the effective slip due to the discretization errors. Obviously, this conclusion signifies the contradiction between the

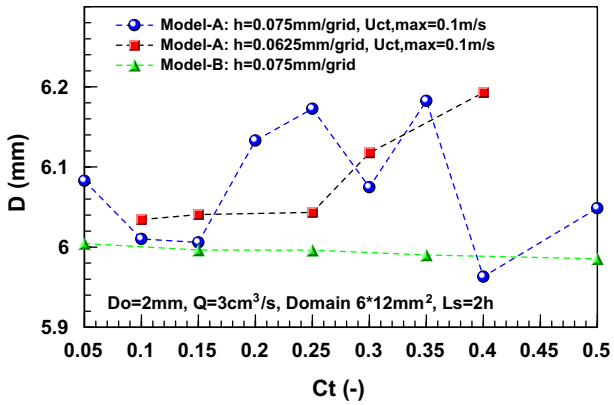

Fig. 7. Effect of time step coefficient.

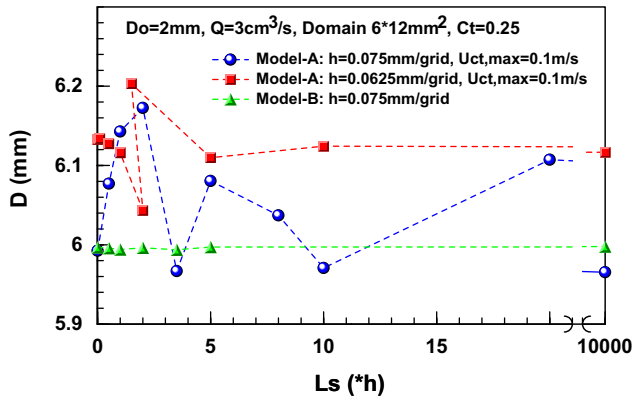

Fig. 8. Effect of slip-length.

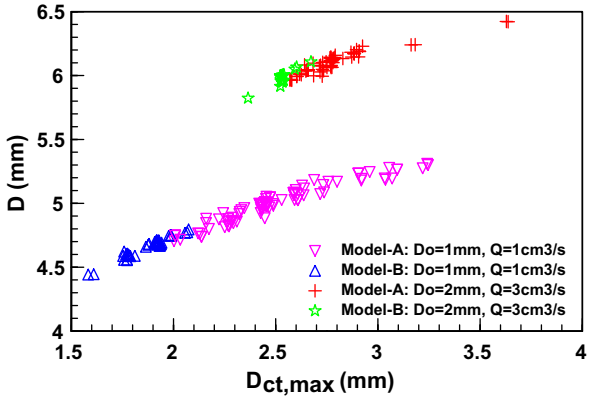

Fig. 10. Bubble departure diameter vs. maximum contact diameter.

macroscopic numerical approach and the physical reality. Since the true slip-length is of the order of intermolecular distance.

3.2.4. Effect of maximum contact line velocity $u_{ct,max}$ (Fig. 9)

The prescribed value of the maximum contact line velocity has a significant effect on the calculated bubble departure diameter by using Model-A (Eq. (7)). Generally, D depends nonlinearly on $u_{ct,max}$ for $u_{ct,max} < 0.25$ m/s; thereafter, it increases linearly with $u_{ct,max}$ and the effects of the grid spacing disappear. Even if we assume that Eq. (7) correctly approximates the relationship between the contact line velocity u_{ct} and the contact angle θ, $u_{ct,max}$ remains as one of the undetermined parameters for Model-A, which has to be determined by experiments for different systems.

3.2.5. Summary and comments

The data shown in Figs. 6–9 are summarized in Fig. 10 as the bubble departure diameter D against the maximum contact diameter $D_{ct,\,max}$. Also shown in the figure are the similar tests carried out for the case $D_o = 1$ mm and $Q = 1$ cm^3/s. A clear tendency can be seen: the departure diameter increases almost linearly with the maximum contact diameter. Thus, we can postulate that the change of the bubble size is realized through the variation of the maximum contact diameter. If $D_{ct,max}$ is (for certain reason) not allowed to be changed, then the impact of the parameters studied in this section would be minimal. This is indeed the case for bubble formations on a thin-walled nozzle with or without liquid co-flow, where the contact line tends to stick on the inner rim of the nozzle and the maximum deviation in bubble departure diameter was found to be less than 1% under various conditions (refer Table 1 in Chen et al. (2008)). It can also be seen from Fig. 10 that, for a given orifice diameter and gas flow rate, the discrepancy of predicted bubble diameters could be very high by using different contact line models and different parameters. This is particularly obvious when Model-A is used.

In summary, for both contact line Model-A and Model-B, the calculated bubble diameters converge to a single value for a relatively small grid spacing (<0.07 mm/grid). For Model-B with $h = 0.075$ mm/grid, an independent calculation result can be achieved with respect to the domain size, the time step size and the slip-length. Similar independences can also be achieved for Model-A with $h = 0.0625$ mm/grid; however, as the grid spacing increases to 0.075 mm/grid, the calculations are found to depend nonlinearly on the above parameters. Compared to Model-B, Model-A shows a more irregular dependence on the boundary conditions and on the slip-length when $L_s < 5$ h.

The above results tend to suggest that, for both Model-A and Model-B, a parameter-independent result can be obtained when the grid spacing is sufficiently small, with a better convergence property for Model-B. In this study, we did not intend to decrease the grid-size further which could require a formidable amount of computation resources for a parameter study like this one. Note that for Model-B, the apparent receding and advancing contact angles are the only input parameters. However, for Model-A, an additional parameter is required, viz. the maximum contact line velocity, which has a significant effect on the predicted bubble diameters (Fig. 9). Basically, the maximum contact line velocity has to be determined by experiments, which is unavailable so far for bubble formation. In this sense, Model-B is superior than Model-A.

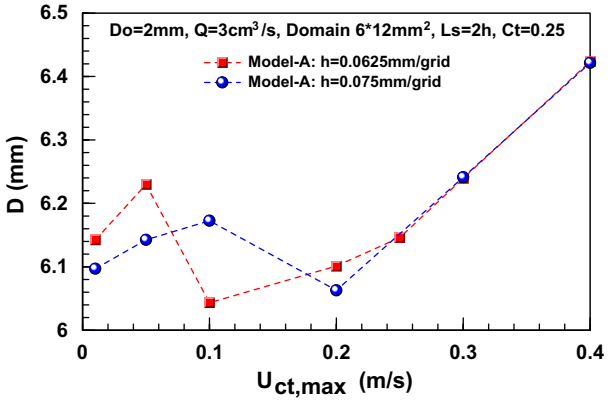

Fig. 9. Effect of maximum contact velocity.

3.3. Effect of contact angles

The effect of contact angles on the bubble departure diameter are studied by varying the prescribed advancing contact angle θ_{ad} and receding angle θ_{re}, and using the contact line Model-B. The wall and side velocity boundary conditions are local-free-slip and symmetric, respectively. It has been verified that the local-free-slip condition on the wall leads to the same results as the Navier-slip condition for Model-B (not shown). The grid spacing is $h = 0.075$ mm/grid, time step coefficient is $C_t = 0.25$. The domain sizes for a orifice diameter of 1, 2 and 3 mm are 8×16, 9×18, 10×20 mm^2, respectively.

3.3.1. Transient behavior

Fig. 11 shows the comparison of the transient behaviors of the contact angle θ and the contact radius R_{ct} for two sets of θ_{ad}/θ_{re}, 50°/40° representing a wetting surface and 110°/70° representing a less wetting surface, respectively. Generally, after the initial

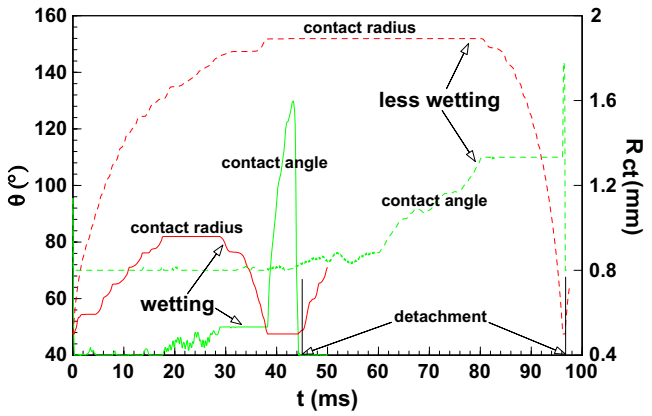

Fig. 11. Transient contact angle and contact radius for a wetting surface ($\theta_{ad} = 50°$, $\theta_{re} = 40°$) and a less wetting surface ($\theta_{ad} = 110°$, $\theta_{re} = 70°$) with $D_o = 1$ mm and $Q = 1$ cm^3/s.

hemispherical bubble is set to grow, the contact angle approaches quickly to the receding angle, and the contact radius expands gradually while the contact angle remains essentially the value of the receding angle. When the contact radius reaches the maximum, it remains constant while the contact angle increases to the value of the advancing angle. Thereafter, the contact line begins to shrink with a constant contact angle until it reaches the inner rim of the orifice mouth. Then the necking process of the bubble starts with a contact angle increasing beyond the advancing angle and detaches thereafter. For both sets of wetting angles, the general behavior of the contact lines is similar. However, the maximum contact radius for the less wetting case is much larger than for the wetting case, resulting in a much bigger bubble diameter (more than doubled in bubble volume). The contact line behavior shown in Fig. 11 is very similar to the experimental results of Schimann (2004) for a static receding angle of 86° and an advancing angle of 104°. Unfortunately, the gas flow rate used by Schimann is not constant, thus a quantitative comparison is not possible (the same holds for the data shown by Gnyloskurenko et al. (2003)). Fig. 12a and b show the bubble contours for the both cases, which are in a qualitative agreement with the visualization results shown in Fig. 1.

3.3.2. Effect of contact angles

The effect of contact angle on bubble departure diameter is shown in Fig. 13. For a mean contact angle of 75°, with increasing the difference ($\theta_{ad} - \theta_{re}$), the departure diameter decreases (Case A). When the receding contact angle is kept constant, the bubble size increases slightly with increasing advancing contact angle (Cases B and C). However, when the advancing angle is kept constant, the bubble size increases significantly with increasing receding contact angle (Cases D and E). By assuming a constant contact angle viz. $\theta_{ad} = \theta_{re}$, the bubble size is found to increase dramatically with increasing contact angle (Case F). In Case F for $D_o = 1$ mm and $Q = 1$ cm^3/s, when the contact angle increases from 40° to 110°, the increase in bubble departure diameter is about 70% which corresponds to an increase of 390% in bubble volume. In fact, in case of an orifice ring (nozzle) with small wall thickness, the contact angle effect can be neglected, as shown in Fig. 14. In this case, the contact line mainly sticks on the inner orifice rim during most of the bubble formation period.

The change of contact angles leads to a change in the maximum contact diameter ($D_{ct,max}$) as shown in Fig. 15. $D_{ct,max}$ is exclusively determined by the receding contact angle. The relationship between $D_{ct,max}$ and θ_{re} is shown in Fig. 16. The ratio $D_{ct,max}/D_o$ increases linearly with θ_{re}. For a very low gas inflow velocity (less than a certain critical value), the contact line tends to stick on the orifice inner rim (viz. $D_{ct,max}/D_o = 1$) for small receding angles (less than a critical value), as shown for the case $D_o = 3$ mm and $Q = 1$ cm^3/s with a gas inlet velocity of 0.14 m/s. In this case, the change of the receding angle has a negligible effect on the bubble departure diameter (refer Fig. 13).

Based on the these results, the bubble departure diameter can be correlated with the receding and advancing contact angles, the orifice diameter and the gas flow rate. However, as discussed above, the use of θ_{re} is not a proper choice, since it needs two critical values (for gas inflow velocity and θ_{re}) which will result in a complicated correlation. Instead, the maximum contact diameter can be used which solely depends on θ_{re} and thus represents the effect of θ_{re}. The relationship can be given as

$$D \sim D_{ct,\,max} Q^{0.4} \theta_{ad}^{0.2}. \tag{10}$$

All variables are dimensional with D and $D_{ct,max}$ in mm, Q in cm^3/s and θ_{ad} in degree. Fig. 17 shows the results. The exponent 0.4 for Q was predicted by Oguz and Prosperetti (1993) for the dynamic growth case considering only the buoyancy and added mass forces.

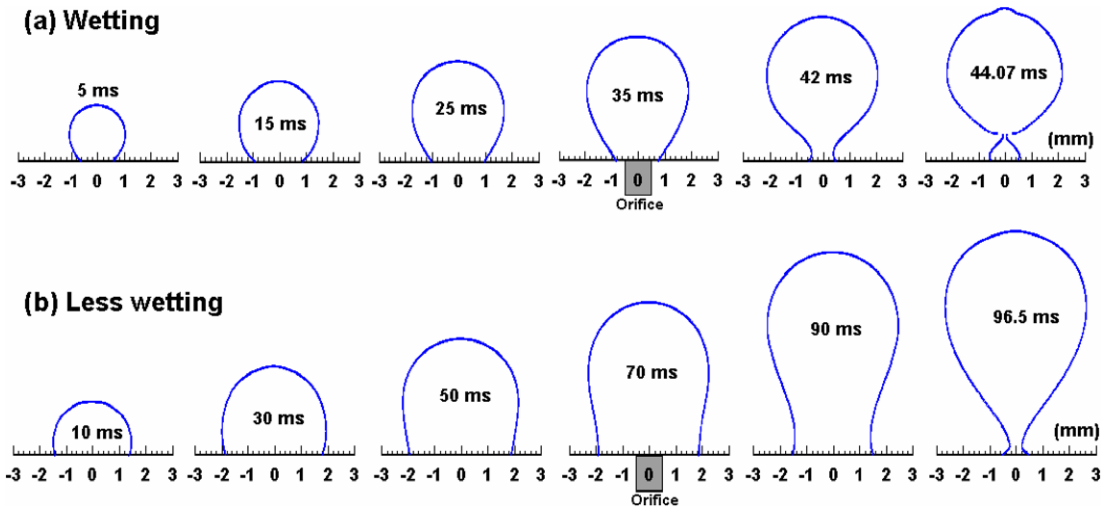

Fig. 12. Bubble contours for a wetting surface ($\theta_{ad} = 50°$, $\theta_{re} = 40°$), (a), and a less wetting surface ($\theta_{ad} = 110°$, $\theta_{re} = 70°$), (b), with $D_o = 1$ mm and $Q = 1$ cm^3/s.

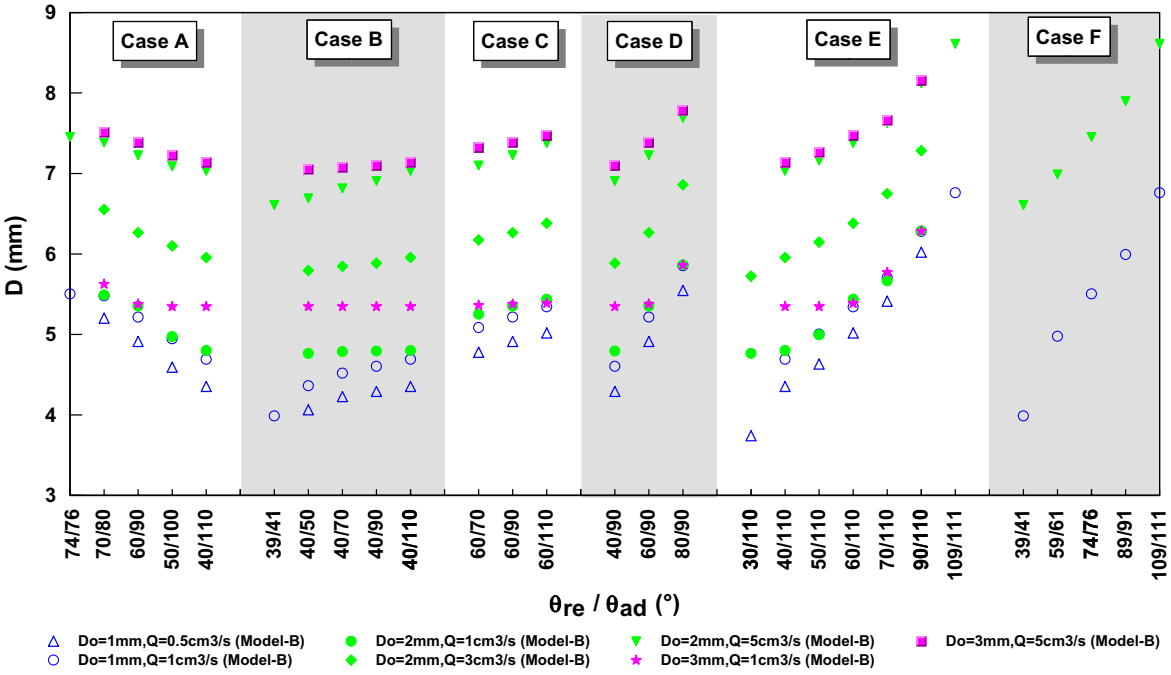

Fig. 13. Effect of advancing and receding contact angles on bubble departure diameter (orifice plate).

From Figs. 16, 17, D is roughly proportional to θ_{re}, provided that $D_{ct,max}/D_o > 1$, while the influence of θ_{ad} is insignificant.

These results show a significant influence of the dynamic contact angles on the macroscopic numerical predictions. By using different contact line models or adopting different sets of the receding and advancing angles, one can obtain a great variety of predictions. Even so, the modeling efforts on the moving contact line beneath a growing bubble should not be stopped. One could, as the first step, generalize a model applicable for a limit class of bubble formation problems, based on the experimental findings on the dynamic contact line and contact angle (similar to the experiments of Bayer and Megaridis (2006) and Blake et al. (1999) on droplets).

3.4. Comparison with experiments

The comparison of calculated (equivalent) bubble departure diameters (of the first and, in some cases, the second detached bubble) with experimental data is shown in Fig. 18. The experimental data are taken from Hsu et al. (2000) (nozzle, N_2/water system), Jamialahmadi et al. (2001) and Ramakrishnan et al. (1969) (orifice plate, air/water system) under constant flow rate condition.

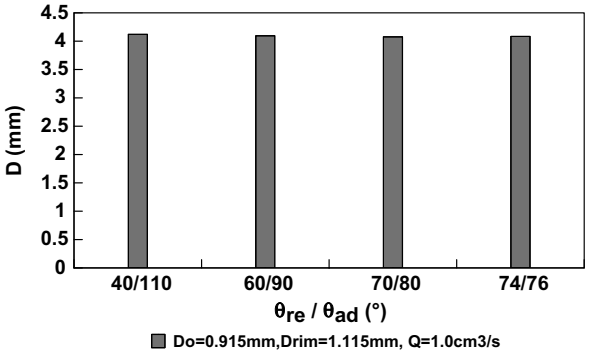

Fig. 14. Effect of advancing and receding contact angles on bubble departure diameter (nozzle).

Model-B is used in these calculations. The wall and side velocity boundary conditions are local-free-slip and symmetric, respectively. The receding contact angle is given as 40° and the advancing contact angle is 90°. The grid spacing is typically 0.075 mm/grid.

Good agreement between calculations and experiments is seen for the orifice diameter of 3 mm (Fig. 18c) and 3.67 mm (Fig. 18d) and particularly for the nozzle case (Fig. 18a) where the contact line movement is limited by the outer rim of the nozzle. For the orifice diameter of 2 mm (Fig. 18b), good agreement is seen for low gas flow rates but the deviation increases for $Q > 3$ cm^3/s. Big deviations exist between experiments and calculations for bubble formation on the orifice plate with $D_o = 1$ mm (Fig. 18a). Furthermore, there is a large difference between the bubble diameters of the first and second detached bubbles. If the calculations are performed for a nozzle with a wall thickness of 0.1 mm, the calculation results agree very well with experiments (cross symbols in Fig. 18a, only two data points available). The mentioned discrepancy can be attributed to the wrong predictions of the contact line behavior (e.g., maximum contact line diameter) by the adopted contact line models. This in turn may be due to the relatively high gas inflow velocity (1.27 m/s), the small bubble size (thus strong capillary force on the contact line), insufficient mesh resolution, or the combination of the above effects.

Fig. 19 shows the variations of the maximum contact diameter with the gas inflow velocity (U_o). For the data which agree well with the experiments, $D_{ct,max}/D_o$ can be well related to U_o, viz., $D_{ct,max}/D_o$ remains 1 for U_o less than 0.6 m/s, then it increases consistently with U_o. Since the bubble departure diameter is strongly influenced by the maximum contact diameter in case that $D_{ct,max}$ is larger than D_o, therefore, U_o could be a key parameter in generating a correlation for bubble departure diameter.

Basically, one can adopt a certain value of θ_{re} and/or θ_{ad} to obtain a calculation result fitting perfectly the experiments. When Model-A is used, an additional adjustable parameter can be used, viz. the maximum contact line velocity. Therefore, it seems meaningless at this stage to compare the simulation results with the experiments in order to justify the numerical scheme or to try to interpret the simulation results without considering the limits of the models

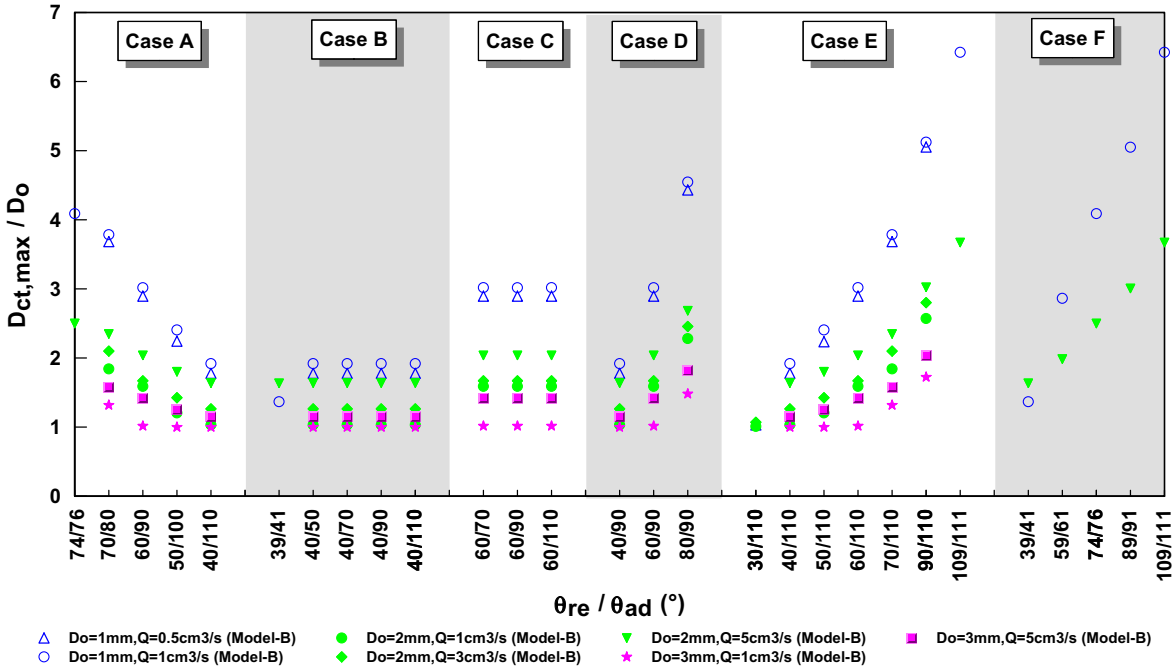

Fig. 15. Effect of advancing and receding contact angles on maximum contact diameter.

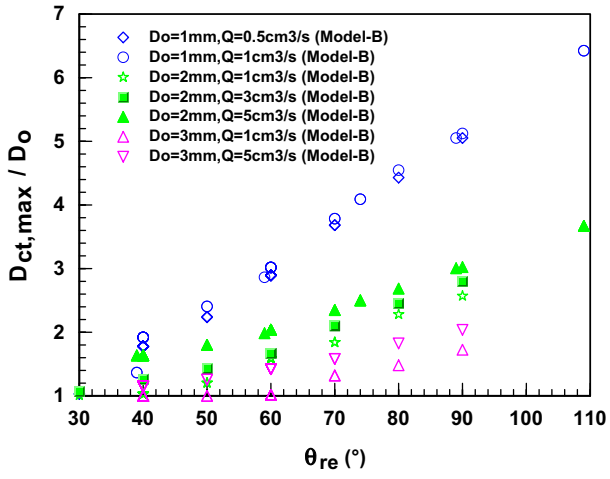

Fig. 16. Maximum contact diameter vs. receding contact angle.

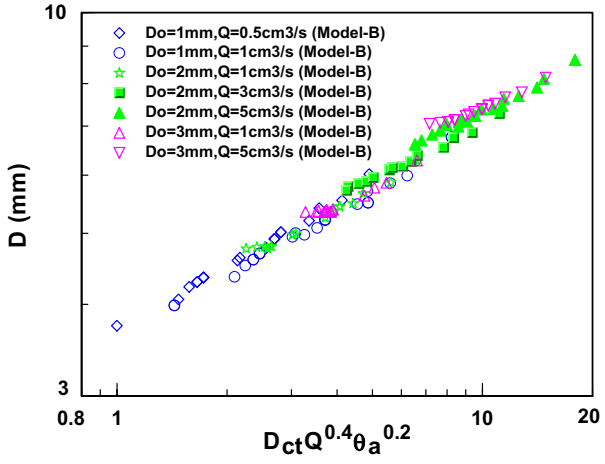

Fig. 17. Correlation of bubble departure diameter.

(this has been done by many researchers). What seems meaningful is that, there exist certain macroscopic rules for the contact line dynamics. In this case, it is found that if a unique set of θ_{re} and θ_{ad} is prescribed, the maximum contact diameter follows a common tendency with regard to the gas flow velocity for various orifice diameters and gas flow rates (Fig. 19). However, it needs to be verified by the experiments whether θ_{re} and θ_{ad} could remain the same for a certain range of operation conditions. In the end, in order to generalize a contact line model for the macroscopic numerical simulations, the experimental data on the dynamic advancing and receding angles and possibly also on the relationship between the dynamic angle and the contact line velocity are essential.

4. Conclusions

In this paper, the effects of the contact angle and the contact line models on the bubble formation from submerged orifices were studied using a 2D axisymmetric numerical scheme involving a level set method for tracking the two-phase interface.

Two kinds of contact line models have been tested. In Model-A (Francois and Shyy, 2003), similar to many other models, the instantaneous apparent contact angle is linearly related to the contact line velocity. In Model-B (stick-slip model), the contact line is set to move only when the contact angle exceeds the range limited by the prescribed receding and advancing angles. For both models, a parameter-independent result could be obtained when the grid spacing is sufficiently small, with a better convergence property for Model-B. For Model-A, besides the receding and advancing angles, an additional parameter needs to be prescribed, viz. the maximum contact line velocity, which has a significant effect on the predicted bubble diameters. Furthermore, compared to Model-B, Model-A shows a more irregular dependence on the boundary conditions and on the slip-length when $L_s < 5h$. Based on these results, Model-B is more reliable than Model-A for the macroscopic simulations.

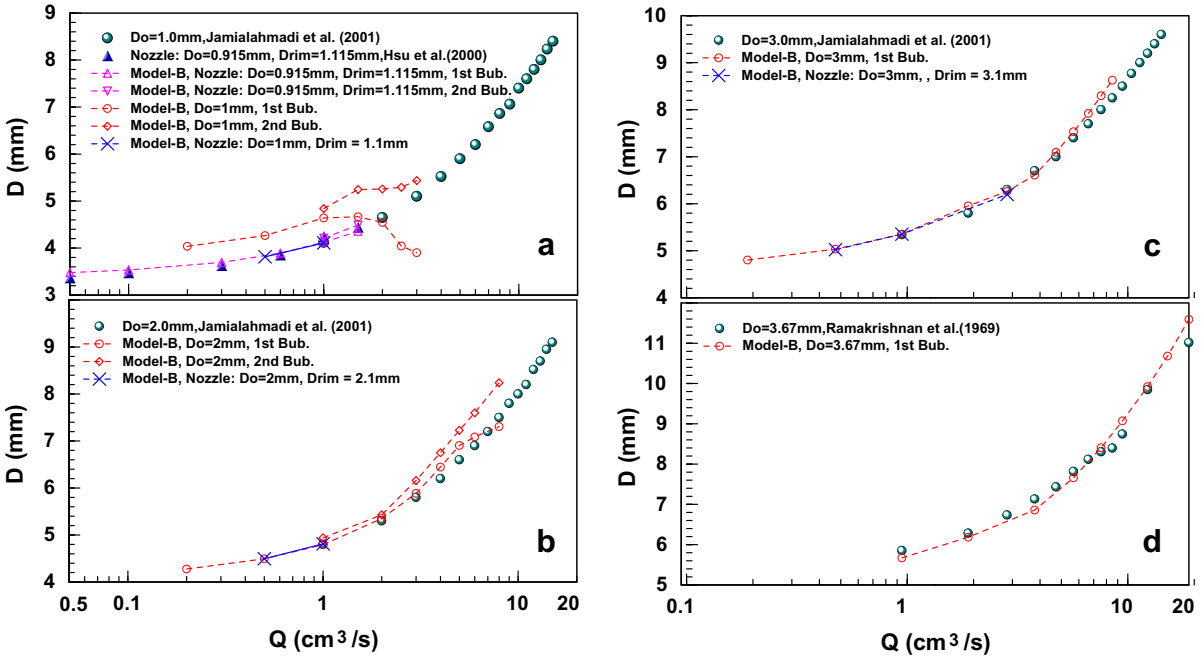

Fig. 18. Comparison of calculated bubble departure diameters with experimental results: (a) D_o = 1.0 mm; (b) D_o = 2.0 mm; (c) D_o = 3.0 mm; (d) D_o = 3.67 mm.

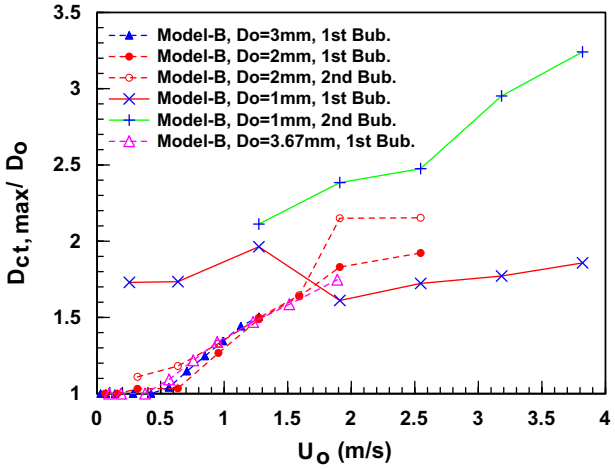

Fig. 19. Maximum contact diameter vs. gas inflow velocity.

The effect of the contact angles on the bubble departure diameter have been studied by varying the prescribed advancing and receding contact angles. The calculated bubble departure diameter increases slightly with the advancing angle, but it increases strongly with the receding angle. The maximum contact diameter is also mainly influenced by the receding contact angle. The bubble departure diameter can be correlated with the maximum contact diameter (representing the effect of receding contact angle), the advancing contact angle, the orifice diameter and the gas flow rate. All parameter dependencies and effects of contact angles tend to disappear when the contact line sticks on the orifice/nozzle mouth, e.g., in case of a nozzle with small wall thickness and/or under liquid co-flow condition.

Due to the strong dependency of the bubble diameter on the prescribed values of the advancing and receding angles and the maximum contact line velocity (in case of Model-A), the comparisons of the calculated bubble departure diameter with experimental data are not very meaningful. Basically, a very good agreement could be obtained by changing any of these input parameters alone. Under the circumstance that a physical boundary condition for the dynamic contact angle is so far unavailable, the experimental data on the dynamic advancing and receding angles and also on the relationship between the dynamic angle and the contact line velocity are urgently needed in order to generalize a contact line model for using in the macroscopic numerical simulations. Not until then, the numerical simulations maybe remain as numerical tests instead of real applications.

References

Bayer, I.S., Megaridis, C.M., 2006. Contact angle dynamics in droplets impacting on flat surfaces with different wetting characteristics. J. Fluid Mech. 558, 415–449.
Blake, T.D., Bracke, M., Shikhmurzaev, Y.D., 1999. Experimental evidence of nonlocal hydrodynamic influence on the dynamic contact angle. Phys. Fluids 11, 1995–2007.
Brackbill, J.U., Kothe, D.B., Zemach, C., 1992. A continuum method for modeling surface tension. J. Comput. Phys. 100, 335–354.
Chen, Y., Kulenovic, R., Mertz, R., 2008. Numerical study on the formation of Taylor bubbles in capillary tubes. Int. J. Thermal Sci. doi:10.1016/j.ijthermalsci.2008.01.004.
Chigarev, N.B., Chigareva, T.S., 1986. Variation of the contact angle in the quasistatic growth of a vapor bubble on a horizontal surface in boiling liquid. J. Eng. Phys. Thermophys. 51, 398–401.
Chorin, A., 1968. Numerical solution of the Navier–Stokes equations. Math. Comp. 22, 745–762.
Cox, R.G., 1986. The dynamics of the spreading of liquids on a solid surface, Part I. Viscous flow. J. Fluids Mech. 168, 169–194.
Diez, J.A., Kondic, L., Bertozzi, A., 2000. Global models for moving contact lines. Phys. Rev. E 63, 011208.
Drelich, J., Miller, J.D., Good, R.J., 1996. The effect of drop (bubble) size on advancing and receding contact angles for heterogeneous and rough solid surfaces as observed with sessile-drop and captive-bubble techniques. J. Colloid Interface Sci. 179, 37–50.
Duhar, G., Colin, C., 2006. Dynamics of bubble growth and detachment in a viscous shear flow. Phys. Fluids 18, 077101.
Dupont, J.B., Legendre, D., Morgante, A.M., 2007. Numerical Simulation of Static or Sliding Drop with Hystersis Contact Line. Sixth Int. Conf. Multiphase Flow. Leipzig, Germany.
Dussan, E.B., Rame, E., Garoff, S., 1991. On identifying the appropriate boundary conditions at a moving contact line: an experimental investigation. J. Fluid Mech. 230, 97–116.
Francois, M., Shyy, W., 2003. Computations of drop dynamics with the immersed boundary method, Part 2: drop impact and heat transfer. Numer. Heat Transfer B 44, 119–143.

Fritz, W., 1935. Berechnung des Maximalvolumens von Dampfblasen. Phys. Z. 36, 379–388.
Fukai, J., Shiiba, Y., Yamamoto, T., et al., 1995. Wetting effects on the spreading of a liquid droplet colliding with a flat surface: experiment and modeling. Phys. Fluids 7, 236–247.
Gelach, D., Alleborn, N., Buwa, V., Durst, F., 2007. Numerical simulation of periodic bubble formation at a submerged orifice with constant gas flow rate. Chem. Eng. Sci. 62, 2109–2125.
Gnyloskurenko, S.V., Byakova, A.V., Raychenko, O.I., Nakamura, T., 2003. Influence of wetting conditions on bubble formation at orifice in an inviscid liquid: transformation of bubble shape and size. Colloids Surf. A 218, 73–87.
Hsu, S.-H., Lee, W.-H., Yang, Y.-M., Chang, C.-H., Maa, J.-R., 2000. Bubble formation at an orifice in surfactant solutions under constant-flow conditions. Ind. Eng. Chem. Res. 39, 1473–1479.
Huang, H., Liang, D., Wetton, B., 2004. Computation of a moving drop/bubble on a solid surface using a front-tracking method. Commun. Math. Sci. 2, 535–552.
Jamialahmadi, M., Zehtaban, M.R., Mueller-Steinhagen, H., Sarrafi, A., Smith, J.M., 2001. Study of bubble formation under constant flow conditions. Trans. IchemE 79, 523–532.
Jensen, M.K., Memmel, G.J., 1986. Evaluation of bubble departure diameter correlations. Eighth Int. Heat Transfer Conf. 4, 1907–1912.
Kalliadasis, S., Chang, H.-C., 1994. Apparent dynamic contact angle of an advancing gas–liquid meniscus. Phys. Fluids 6, 12–23.
Kandlikar, S.G., Steinke, M.E., 2002. Contact angle and interface behavior during rapid evaporation of liquid on a heated surface. Int. J. Heat Mass Transfer 45, 3771–3780.
Kistler, S.F., 1993. Hydrodynamics of wetting. In: Berg, J.C. (Ed.), Wettability. Marcel Dekker, New York, p. 311.
Liow, J.-L., Gray, N.B., 1988. A model of bubble growth in wetting and non-wetting liquids. Chem. Eng. Sci. 43, 3129–3139.
Marmur, A., Rubin, E., 1973. Equilibrium shapes and quasi-static formation of bubbles at submerged orifices. Chem. Eng. Sci. 28, 1455–1464.
Marmur, A., Rubin, E., 1976. A theoretical model for bubble formation at an orifice submerged in an inviscid liquid. Chem. Eng. Sci. 31, 453–463.
Mazouchi, A., Gramlich, C.M., Homsy, G.M., 2004. Time-dependent free surface Stokes flow with a moving contact line, I. Flow over plane surfaces. Phys. Fluids 16, 1647–1659.
Mukherjee, A., Kandlikar, S.G., 2007. Numerical study of single bubbles with dynamic contact angle during nucleate pool boiling. Int. J. Heat Mass Transfer 50, 127–138.
Oguz, H.N., Prosperetti, A., 1993. Dynamics of bubble growth and detachment from a needle. J. Fluid Mech. 257, 111–145.
Osher, S., Sethian, J.A., 1988. Fronts propagating with curvature-dependent speed: algorithms based on Hamilton–Jacobi formulations. J. Comput. Phys. 79, 12–49.
Pasandideh-Fard, M., Qiao, Y.M., Chandra, S., Mostaghimi, J., 1996. Capillary effects during droplet impact on a solid surface. Phys. Fluids 8, 650–659.
Ramakrishnan, S., Kumar, R., Kuloor, N.R., 1969. Studies in bubble formation – I Bubble formation under constant flow conditions. Chem. Eng. Sci. 24, 731–747.
Renardy, M., Renardy, Y., Li, J., 2001. Numerical simulation of moving contact line problems using a volume-of-fluid method. J. Comput. Phys. 171, 243–263.
Schimann, H.C.R., 2004. Force and Energy Measurement of Bubble-Particle Detachment. Master Thesis. Virginia Polytechnic Institute and State University.
Shikhmurzaev, Y.D., 1997. Moving contact lines in liquid/liquid/solid systems. J. Fluid Mech. 334, 211–249.
Shu, C.-W., 2003. High-order finite difference and finite volume WENO schemes and discontinuous Galerkin methods for CFD. Int. J. Comput. Fluid Dyn. 17, 107–118.
Sikalo, S., Wilhelm, H.D., Roisman, I.V., Jakirlic, S., Tropea, C., 2005. Dynamic contact angle of spreading droplets: experiments and simulations. Phys. Fluids 17, 062103.
Smith, K.A., Ottino, J.M., Warren, P.B., 2005. Simple representation of contact-line dynamics in a level-set model of an immiscible fluid interface. Ind. Eng. Chem. Res. 44, 1194–1198.
Somalinga, S., Bose, A., 2000. Numerical investigation of boundary conditions for moving contact line problems. Phys. Fluids 12, 499–510.
Son, G., Dhir, V.K., Ramanujapu, N., 1999. Dynamics and heat transfer associated with a single bubble during nucleate boiling on a horizontal surface. J. Heat Transfer 121, 623–631.
Spelt, P.D.M., 2005. A level-set approach for simulations of flows with multiple moving contact lines with hysteresis. J. Comput. Phys. 207, 389–404.
Stephan, P., Hammer, J., 1994. A new model for nucleate boiling heat transfer. Wärme Stoffübertrag. 30, 119–125.
Stoev, K., Rame, E., Leonhardt, T., Garoff, S., 1998. The effects of thin films on the hydrodynamics near moving contact lines. Phys. Fluids 10, 1793–1803.
Sussman, M., Fatemi, E., 1999. An efficient, interface preserving level set re-distancing algorithm and its application to interfacial incompressible flow. SIAM J. Sci. Comp. 20, 1165–1191.
Xiao, Z., Tan, R.B.H., 2005. An improvement model for bubble formation using the boundary-integral method. Chem. Eng. Sci. 60, 179–186.